Article

Numerical Simulation of the Slag Splashing Process in A 120 Ton Top-Blown Converter

Guang Yang, Baokuan Li *, Meijia Sun, Deyue Qin and Liangcai Zhong

School of Metallurgy, Northeastern University, Shenyang 110819, China; 2071722@stu.neu.edu.cn (G.Y.); sunmj@mail.neu.edu.cn (M.S.); 2210684@stu.neu.edu.cn (D.Q.); zhonglc@mail.neu.edu.cn (L.Z.)
* Correspondence: libk@smm.neu.edu.cn

Abstract: Slag splashing operations at the end of the converter blow process can improve the furnace liner life and the converter operation rate. However, the effect of factors on slag splashing at actual dimensions is yet to be fully understood. A three-dimensional transient mathematical model coupled with the response surface analysis has been established to investigate the effects of the amount of remaining slag, oxygen lance height, and top-blowing nitrogen flowrate on the slag splashing process in a 120 ton top-blown converter. The predicted splashing density is validated by the experimental data. The numerical simulation results show that the splashing density and the splashing area ratio increase with the amount of remaining slag, which has the greatest effect on slag splashing. As the oxygen lance height decreases, the splashing density and the splashing area ratio first increase and then decrease. The top-blowing nitrogen flowrate is positively correlated with the splashing area ratio. When the oxygen lance height is high, the impact of the top-blowing nitrogen flowrate on the splashing density is not significant. The splashing density increases with increasing top-blowing nitrogen flowrate as the oxygen lance height is low.

Keywords: top-blown converter; slag splashing; numerical simulation; response surface analysis

1. Introduction

Slag splashing technology is widely used for protecting the refractory and increasing the life of the converter liner [1–4]. The slag splashing process involves adding a slag regulator to the slag that remains at the bottom of the converter after the molten steel has been poured into the ladle. This is performed in order to improve the slag's ability to stick to the refractory surface of the converter liner. The supersonic nitrogen jets into the slag pool as the height of the oxygen lance decreases. The slag splashes onto the refractory surface to form a protective slag layer for protecting the refractory surface and improving the lifespan of the furnace. It takes 2 to 4 min to complete the splashing process. Finally, the remaining slag should be poured out the furnace bottom to prevent blockage of the bottom blow nozzle. The slag droplets are separated from the slag pool through the impact of a high-speed nitrogen jet and subsequently splashed onto the converter liner. The effect of slag splashing is primarily influenced by some factors such as the height of the oxygen lance, the rate of nitrogen flow, the amount of remaining slag, and the angle of the oxygen lance nozzle.

To begin with, it is important to understand the mechanism behind the slag splashing process. Li et al. [5] investigated the phenomenon of metal droplet splashing during the blowing process using numerical simulations. They identified two mechanisms responsible for splash generation: the direct exclusion of individual droplets from the edge of the impact pit, and the formation of "splash sheets" or "large tears," which are broken and torn into small droplets of varying sizes by the reflective flow at the edge of the impact pit. Zhang et al. [6] found that the impact cavity shape gradually changed following the sequence of "disc" → "bowl" → "cone" with an increase in the gas flow, leading to the

variation in the splashing modes. Feng et al. [7] studied the collision process between molten particles and a wall and investigated the effects of particle diameter, initial temperature, and impact velocity, as well as the initial temperature of the wall, on the process. They found that individual particles undergo spreading, retracting, and stabilizing processes when they impact the wall. Liu et al. [8] analyzed the energy transfer efficiency of the top-blown gas to the molten pool through numerical simulations. They calculated the energy consumption of the splashing process and established the energy conservation equation in the blowing process. Yuan et al. [9] measured the wettability between molten slag and MgO-C refractory by wetting experiments to demonstrate the mechanism of slag adhesion and protection mechanism during slag splashing. According to Chen et al. [10], modified vanadium slag demonstrated excellent fluidity and adhesion, facilitating normal slag splashing operations that help reduce the erosion of the vanadium converter liner.

The splashing effect is mainly related to the oxygen lance position, blowing nitrogen flowrate, the amount of remaining slag, slag properties and the top lance nozzle angle [11,12]. Tao et al. [13] conducted water-mode experiments to study the distribution of slag splash in different parts of the converter liner and the effects of oxygen lance position, the amount of remaining slag, and gas pressure on slag splash. They determined the optimal values for each parameter. Wang et al. [14] conducted a physical modeling of the slag splashing practice in an 80 ton combined-blown converter and obtained the influence significance of different operating parameters on slag splashing by ANOVA. Zou et al. [15] studied the melt splashing behavior in the smelting process of oxygen-enriched side-blown furnaces and found that reducing the injection speed, increasing the lance immersion depth, and increasing the liquid level can decrease the splashing height. Mills et al. [16] found that slag splashing involves both "slag wash coating" and "slag ejection coating" mechanisms. They discovered that in addition to top-blowing flowrate, oxygen lance height, oxygen lance angle, and slag pool depth, the influence of slag physical parameters on the effect of splashing is also important. Sinelnikov et al. [17] calculated and simulated the splashing process to determine the factors affecting splashing. They found that optimizing the flowrate, pressure and temperature of the nitrogen jet, the height and angle of the oxygen lance, the depth of the jet into the slag layer, and the consumption of MgO can improve the splashing efficiency. The numerical simulation results were in agreement with the experimental results of the physical model. Leão et al. [18] performed transient simulations of slag splashing behavior using Fluent to investigate the effects of fluid temperature, density, viscosity, and interfacial tension on the effect of slag splashing. Cao et al. [19] analyzed the multiphase interaction behavior of a supersonic oxygen jet impinging on a free interface by numerical simulation and found that slag viscosity and surface tension have little effect on the generation rate of splashing droplets.

There are also a number of scholars who have innovated slag splashing technology. In a study by Zhang et al. [20], the use of CO_2 instead of N_2 in the splashing process was investigated through numerical simulations. They compared the performance of a five-nozzle oxygen lance with a central nozzle to that of a conventional four-nozzle oxygen lance and found that improving CO_2 jet performance is possible by reducing the axial distance, increasing CO_2 stagnation pressure, and increasing CO_2 preheating temperature. Zhao et al. [21] developed a new method to separate and recover CO_2 from exhaust gas for slag splashing. They calculated the equilibrium conversion rate of CO_2 slag splashing under different process conditions using enthalpy, entropy, and heat capacity procedures, and analyzed the factors affecting CO_2 slag splashing. In another study, Sinelnikov et al. [22] investigated the slag splashing process in oxygen converters through numerical simulation. They found that heating the top-blown nitrogen and increasing the gas temperature in the converter can enhance the slag-splashing ability of supersonic jets. Kalinogorskii et al. [23] analyzed the slag droplet motion in the converter by numerical modeling, refined the description of the slag droplet motion in the splashing process, and established the relation between the parameters of the slag droplet motion and the characteristics of the swirling jet.

Previous scholars have made significant contributions to the study of slag splashing processes. Currently, water model experiments still dominate the study of slag splashing processes, while numerical simulation studies are less common. The numerical simulation method is a fast and efficient approach to capture physical quantities that are often challenging to obtain through experimental methods, such as the temperature distribution of the slag, the velocity vector of the gas, and even the trajectory and number of splashing droplets. Moreover, this method is highly controllable and provides excellent visualization of the calculation results [24]. To address the issue of slag adhesion to the converter liner, it is common practice to place absorbent cotton near the converter liner or create grooves in the liner surface. Hence, the splashed slag can be absorbed by the absorbent cotton or caught by the grooves to avoid flowing back to the converter bottom. However, these methods change the surface characteristics and geometric structure of the furnace liner. The precise distribution of slag that adheres to the converter liner cannot be revealed clearly. This paper presents a three-dimensional transient mathematical model of the slag splashing process in a 120 ton top-blown converter. The splashed slag droplets adhere to the converter liner and spread out to form a film at the impact point by the user-defined function (UDF). A parametric analysis is conducted to investigate three primary factors—the amount of remaining slag, oxygen lance height, and top-blowing nitrogen flowrate—that influence the effect of slag splashing. Furthermore, response surface optimization is utilized to predict the optimal range of operating parameters.

2. Mathematical Model

2.1. Basic Assumptions

Given the complexity of the slag splashing process in actual operations, certain simplifications and assumptions are employed during the simulation process:

1. Nitrogen is considered as an ideal gas and the slag is considered as an incompressible fluid.
2. The physical parameters of slag remain constant regardless of temperature except for viscosity.
3. It is believed that once the slag comes into contact with the converter liner, it immediately adheres to the surface of the furnace liner.

2.2. Governing Equations

Slag splashing is a complex multiphase flow process that encompasses gas jets, fluctuations at the gas–liquid interface, and slag droplet motion. There is an obvious interface between the gas–slag phase.

In the present study, the VOF (volume of fluid) model is used to solve the gas–slag interface due to its ability to accurately trace the free boundary of two-phase or multiphase incompatible fluids with no significant drawbacks [25–29].

In the VOF model, the nitrogen is set as the primary phase and the slag as the secondary phase. The distribution of the volume fraction for each phase and the tracking of the phase interface is accomplished by solving the continuity equation for the volume fraction of the slag α_{slag}:

$$\frac{\partial \alpha_{\text{slag}}}{\partial t} + \nabla \cdot \left(\alpha_{\text{slag}} \overrightarrow{u} \right) = 0 \tag{1}$$

where $\overrightarrow{u}$ is the velocity vector, m·s^{-1}. The volume fraction of the nitrogen α_{nitrogen} will be determined by the phase continuity constraint: $\alpha_{\text{nitrogen}} = 1 - \alpha_{\text{slag}}$.

The mass equation, momentum equation and energy equation in VOF are shown below.
Mass equation:

$$\frac{\partial \rho}{\partial t} + \nabla \cdot \left(\rho \overrightarrow{u} \right) = 0 \tag{2}$$

Momentum equation:

$$\frac{\partial}{\partial t}\left(\rho \vec{u}\right) + \nabla\left(\rho \vec{u}\vec{u}\right) = -\nabla p + \nabla \cdot \left[\mu_{eff}\left(\nabla \vec{u} + \nabla \vec{u}^T\right)\right] + \rho \vec{g} + f_\sigma \tag{3}$$

where $\vec{u}$ is the velocity vector, m·s^{-1}; p is the pressure, Pa; $\vec{g}$ is the gravitational acceleration vector, m·s^{-2}; ρ is the density, kg·m^{-3}; f_σ is the surface tension, N·m^{-3}; μ_{eff} is the effective viscosity, Pa·s, $\mu_{eff} = \mu + \mu_t$.

The flow variable field and physical properties are obtained by averaging of each phase:

$$\rho = \alpha_{\text{nitrogen}}\rho_{\text{nitrogen}} + \alpha_{\text{slag}}\rho_{\text{slag}} \tag{4}$$

$$\mu = \alpha_{\text{nitrogen}}\mu_{\text{nitrogen}} + \alpha_{\text{slag}}\mu_{\text{slag}} \tag{5}$$

where the density of nitrogen gas satisfies the ideal gas equation of state.

$$\rho_{\text{nitrogen}} = \frac{p}{RT} \tag{6}$$

Energy equation:

$$\frac{\partial(\rho E)}{\partial t} + \nabla \cdot \left[\vec{u}\left(\rho E + p\right)\right] = \nabla \cdot \left(\lambda_{eff}\nabla T\right) + S_h \tag{7}$$

where S_h represents radiation and other volume heat sources, W·m^{-1}; T is the temperature; λ_{eff} is the effective thermal conductivity, W·m^{-1}·K^{-1}, $\lambda_{eff} = \lambda + \lambda_t$. T and λ are shared by all phases and obtained by averaging the volumes of all phases.

$$T = \alpha_{\text{nitrogen}}T_{\text{nitrogen}} + \alpha_{\text{slag}}T_{\text{slag}} \tag{8}$$

$$\lambda = \alpha_{\text{nitrogen}}\lambda_{\text{nitrogen}} + \alpha_{\text{slag}}\lambda_{\text{slag}} \tag{9}$$

The energy E is obtained by averaging the mass of each phase:

$$E = \frac{\alpha_{\text{nitrogen}}\rho_{\text{nitrogen}}E_{\text{nitrogen}} + \alpha_{\text{slag}}\rho_{\text{slag}}E_{\text{slag}}}{\alpha_{\text{nitrogen}}\rho_{\text{nitrogen}} + \alpha_{\text{slag}}\rho_{\text{slag}}} \tag{10}$$

For the description of the turbulent motion of the converter splashing process, there is no two-equation turbulence model that can be applied to all phases simultaneously. Considering the calculation accuracy and calculation quantity, the realizable k-ε turbulence model is used to calculate turbulent motion [30–35], where the turbulent flow energy k and the turbulent dissipation rate ε can be expressed as:

$$\frac{\partial}{\partial t}(\rho k) + \frac{\partial}{\partial x_j}(\rho k u_j) = \frac{\partial}{\partial x_j}\left[\left(\mu + \frac{\mu_t}{\sigma_k}\right)\frac{\partial k}{\partial x_j}\right] + G_k + G_b - \rho\varepsilon - Y_M \tag{11}$$

$$\frac{\partial}{\partial t}(\rho\varepsilon) + \frac{\partial}{\partial x_j}(\rho\varepsilon u_j) = \frac{\partial}{\partial x_j}\left[\left(\mu + \frac{\mu_t}{\sigma_\varepsilon}\right)\frac{\partial\varepsilon}{\partial x_j}\right] + \rho C_1 S\varepsilon - \rho C_2\frac{\varepsilon^2}{k + \sqrt{v\varepsilon}} + C_{1\varepsilon}\frac{\varepsilon}{k}C_{3\varepsilon}G_b \tag{12}$$

where G_k and G_b are the turbulent kinetic energy generated by the mean velocity gradient and buoyancy, respectively, kg·m^{-1}·s^{-3}. Y_M is the effect of compressible turbulent pulsating expansion on the total dissipation rate, for incompressible fluid (slag), $Y_M = 0$, $Y_M = 2\rho\varepsilon M_t^2$. $C_{1\varepsilon}$, C_2, the turbulent Planter number σ_ε of ε and the turbulent Prandtl number σ_k of k are constant, with values of 1.44, 1.9, 1.2 and 1.0, respectively. The rest of the variables can be calculated by the following equation.

$$\begin{cases} C_1 = \max\left[0.43, \frac{\eta}{\eta+5}\right] \\ \eta = \sqrt{2S_{ij} \cdot S_{ij}}\frac{k}{\varepsilon} \\ S_{ij} = \frac{1}{2}\left(\frac{\partial u_i}{\partial x_j} + \frac{\partial u_j}{\partial x_i}\right) \\ \mu t = \rho C_\mu \frac{k_2}{\varepsilon} \end{cases} \quad (13)$$

where

$$\begin{cases} C_\mu = \frac{1}{A_0 + A_s U^* k/\varepsilon} \\ A_0 = 4.0 \\ A_s = \sqrt{6}\cos\phi \\ \phi = \frac{1}{3}\cos^{-1}\left(\sqrt{6}W\right) \\ W = \frac{S_{ij}S_{jk}S_{kj}}{\sqrt{S_{ij} \cdot S_{ij}}} \\ U^* = \sqrt{S_{ij}S_{ij} + \Omega_{ij}\Omega_{ij}} \end{cases} \quad (14)$$

where Ω_{ij} is the velocity tensor in a rotating flow field, and $\Omega_{ij} = 0$ in this model because the flow field is non-rotating.

3. Numerical Simulation Details

3.1. Physical Model and Meshing

Figure 1 shows a cross-sectional view of a 120 ton converter in a steel mill and the four-nozzle oxygen lance. The geometric parameters of the 120 ton converter and the oxygen lance nozzle are presented in Table 1.
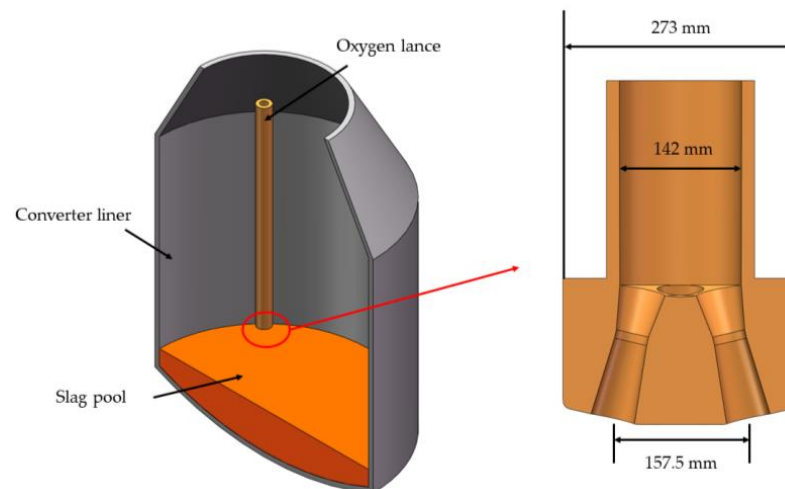
Figure 1. Cross-sectional view of a 120 ton converter and the four-nozzle oxygen lance.

Table 1. The geometric parameters of the 120 ton converter and the oxygen lance nozzle.

Geometric Parameters	Value
Nozzle inlet diameter/(mm)	54
Nozzle throat diameter/(mm)	38.5
Nozzle outlet diameter/(mm)	52
Length of shrink section/(mm)	51.5
Length of throat section/(mm)	10
Length of expansion section/(mm)	92
Nozzle angle/(°)	13
Converter diameter/(mm)	4660
Melting pool depth/(mm)	1258

The computational domain of the 120 ton converter and oxygen lance is discretized by a polyhedral mesh with a hexahedron core, as illustrated in Figure 2. Taking into account the calculation accuracy and cost, the final decision on the mesh number is around 1.2 million.
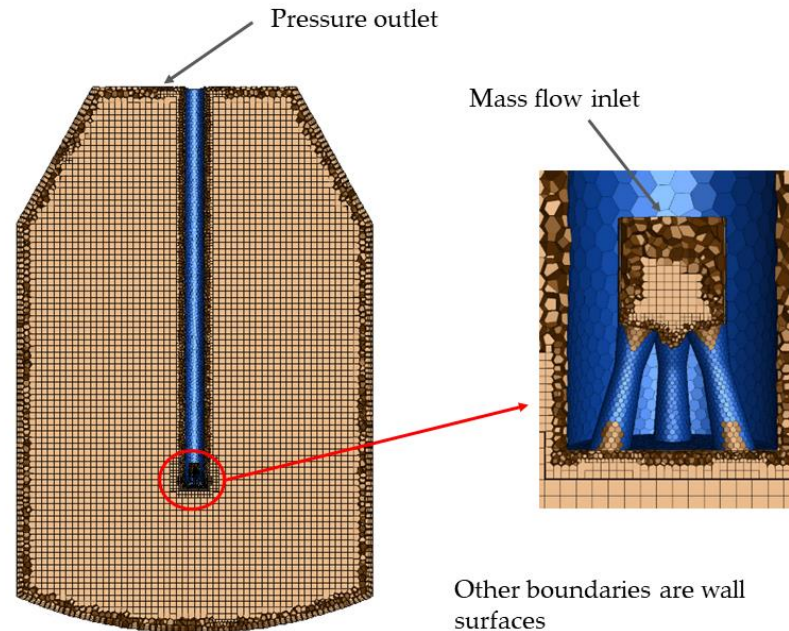
Figure 2. Schematic diagram of mesh division.

3.2. Physical Parameters

In the actual splashing process, the slag droplets are difficult to splash with a large viscosity, when the slag viscosity is too large, it can make the slag droplets difficult to splash up, resulting in a poor splashing effect. Conversely, when the slag viscosity is too small, the slag droplets may not adhere firmly to the converter liner surface after splashing, leading to a flow back to the slag pool along the converter liner surface. Therefore, during the splashing process, a slag regulator is usually added to the remaining slag for increasing the sensitivity of slag viscosity to temperature changes. This ensures that slag droplets can splash easily, and adhere more firmly to the converter liner by becoming tacky quickly.

The decrease in temperature leads to the supersaturation of CaO and MgO with higher melting points in the slag, thereby resulting in their precipitation in the form of solid particles [36]. This increases slag friction and leads to an increase in slag viscosity. As the solidification of slag is not considered in this paper, the impact of the solid fraction on the effective viscosity of slag is incorporated into the effect of temperature on its effective viscosity. This paper assumes that the effective viscosity of slag varies with temperature as shown in Figure 3. The physical parameters employed in this study are presented in Table 2.

3.3. Boundary Conditions

The boundary conditions of the slag splashing process are shown in Table 3. The standard wall function method is used near the wall in the turbulence model, and the wall surface does not slip.

Referring to Figure 4, an annulus region is established in close proximity to the converter liner. Slag droplets entering this region are regarded as adhering to the liner. The thickness of the annulus is small enough in relation to the converter's diameter—approximately 0.3%—that has no impact on the splashing of slag droplets within the converter. The slag droplets spread out slightly and form a film around the impact points on the converter liner surface due to a high velocity. In this paper, the UDF is employed to ensure that the vertical velocity of the slag droplet is defined as 0 once they

have completely entered the annular region near the converter liner. This measure makes the slag droplets adhere to the converter liner and prevents them from falling back into the slag pool.
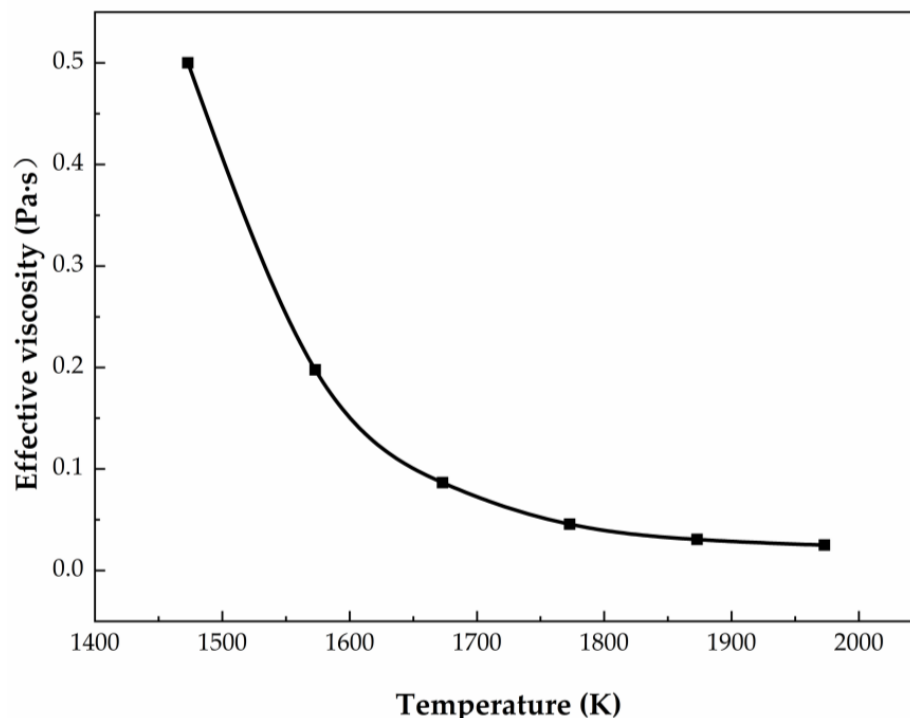
Figure 3. Variation in the effective viscosity of slag with temperature.

Table 2. Physical parameters of slag splashing process.

Material Properties	Slag	Nitrogen
Density/(kg·m^{-3})	3000	ideal-gas
Effective viscosity/(Pa·s)	0.025~0.5	1.663×10^{-5}
Surface tension coefficient/(N·m^{-1})	0.54	-
Specific heat/(j·kg^{-1}·k^{-1})	1200	1040.67
Thermal conductivity/(W·m^{-1}·K^{-1})	1.7	0.0242

Table 3. Boundary conditions.

Boundary Conditions	Value
Converter outlet pressure/(Pa)	101,325
Converter furnace pressure/(Pa)	101,325
Inlet nitrogen temperature/(K)	300
Converter furnace temperature/(K)	1873
Slag pool temperature/(K)	1923
Oxygen lance height/(mm)	1100, 1500, 1900
Mass flowrate of nitrogen/(kg·s^{-1})	13.194, 13.889, 14.583
Amount of remaining slag/(%)	6, 9, 12
Temperature of the converter liner and cap/(K)	1473
Other wall surfaces/(K)	Adiabatic

The SIMPLE scheme is for the pressure-velocity coupling of the gas–liquid flow. Considering the computational speed and computational stability, the pressure interpolation adopts Pressure Staggering Option discrete format. The Compressive Interface-Capturing Scheme for Arbitrary Meshes format is used for the interpolation of free interfaces. This interpolation format is particularly suitable for cases with high viscosity ratios between

fluids, and can capture sharp free interfaces with the same interpolation accuracy as the Geometric Reconstruction format [37]. The transport equations are discretized for the convective terms using a Second Order Upwind. The initial time step is set to 2×10^{-5} s, and subsequent calculations automatically adjust the time step according to the restriction that the Courant number is less than 5. The calculation converges when the energy residuals are less than 10^{-6} and the residuals of other variables are less than 10^{-5}.
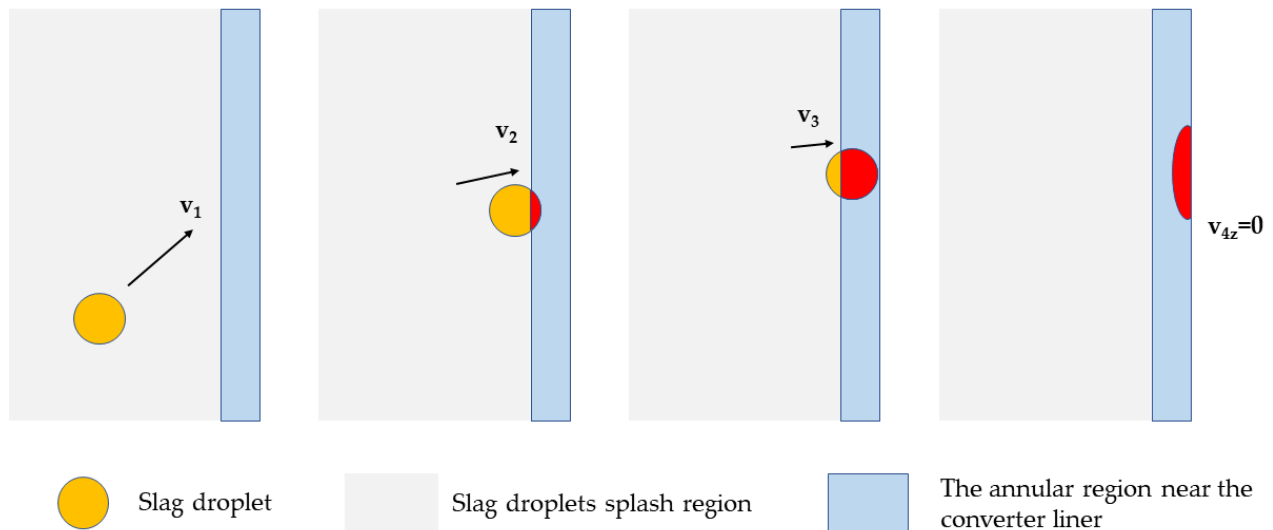
Figure 4. Schematic diagram of slag droplet adherence to converter liner.

4. Results and Discussion

4.1. Model Validation

Water model experiments are conducted using a 1:10 scaled model of the 120 ton converter. Figure 5 shows the schematic diagram of the apparatus in physical modeling. Equal modified Froude numbers of the prototype and water model are used as the main kinetic similarity conditions. An aqueous glycerol solution in the ratio of 10:3 is used to simulate the slag in the experiment, so that the solution has a suitable kinematic viscosity to effectively simulate the effect of slag splashing. Compressed air is selected to simulate the nitrogen injected into the converter. The inner wall of the model converter is hung with sampling grooves at different height intervals to receive the solution splashed onto the inner wall of the converter. After splashing, the splash density is calculated for different height intervals based on the mass of the aqueous glycerol solution in the sampling groove and the splash time.

The numerical simulation is conducted with the same physical parameters and boundary conditions consistent with that in the water model. Figure 6 compares the splashing density at different height intervals on the inner wall of the converter between the water model experiment and numerical simulation. The splashing density refers to the amount of splashed slag liquid onto the wall per unit of internal surface area and per unit of time. The predicted splashing density is in general agreement with the experimental data for confirming the reliability of the mathematical model.

4.2. Numerical Result of Slag Splashing

In the present work, a suitable time point as a criterion is selected to analyze the splashing density and evaluate the slag splashing effect. Figure 7 demonstrates the splashing density variation over time with the amount of remaining slag at 12%, oxygen lance height of 1900 mm, and a top-blowing nitrogen flowrate of 40,000 $\text{Nm}^3 \cdot \text{h}^{-1}$. The fluctuation of the splashing density presents a significant oscillation in the initial stage of the splashing process as the nitrogen jet impacts the slag pool for generating an impact crater. At this stage, the slag pool's liquid level fluctuates heavily, and the randomness of the splashing

situation of slag droplets is high. As the splashing time increases, the variation in the splashing density levels off at approximately 10 s. To balance the calculation time and the predicted splashing density reasonability, the statistical time point of 10 s in the slag splashing process is selected for the response surface analysis in each working condition.
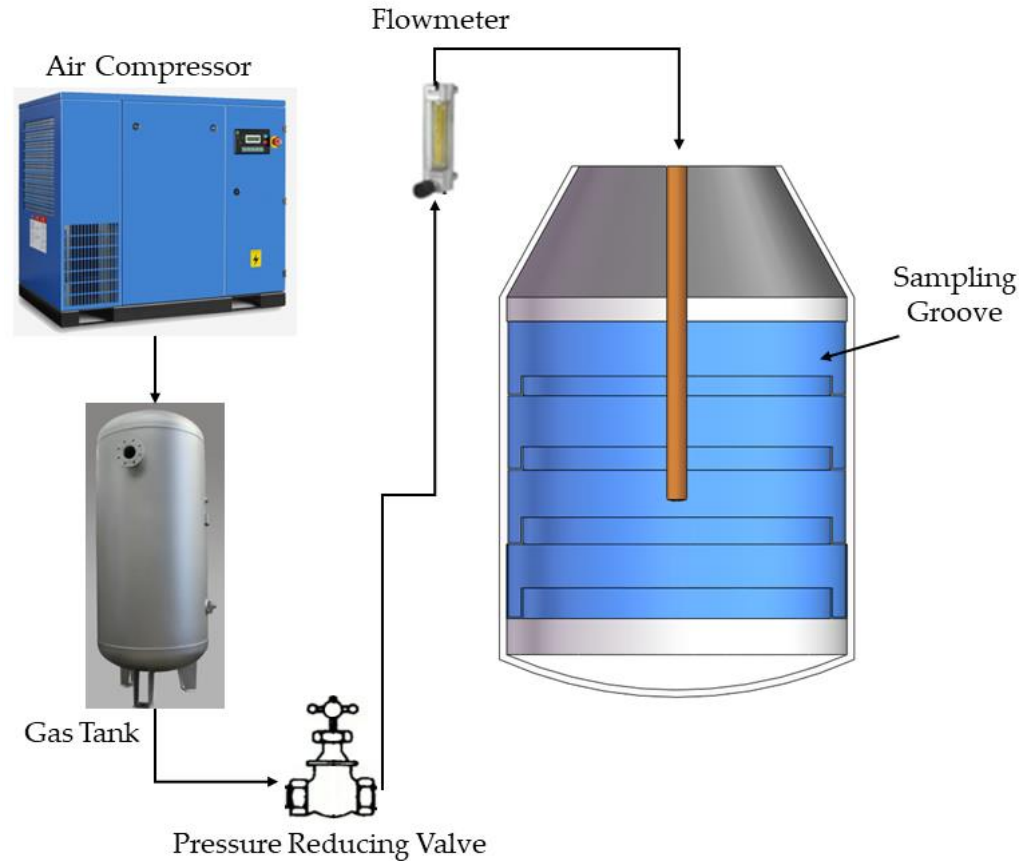
Figure 5. Schematic diagram of the apparatus in physical modeling.
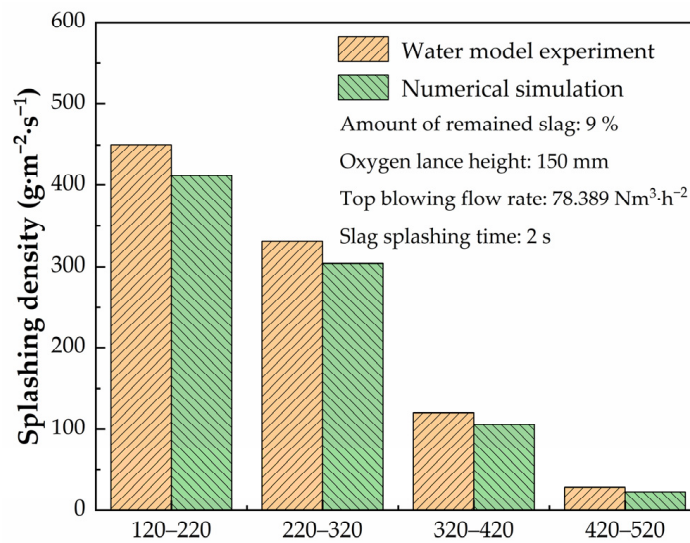
Height intervals from the bottom of the converter model (mm)

Figure 6. The splashing density at different height intervals on the inner wall of the converter model.
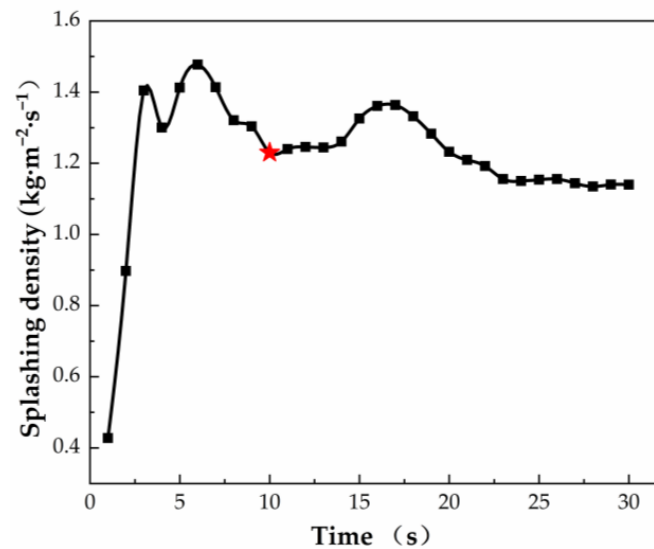
Figure 7. The variation trend of the splashing density over time.

Figure 8 shows the cross-sectional view of the phase distribution when the splashing process lasts for 30 s. It can be observed that the slag at the bottom of the converter is splashed up due to the impact of the top-blowing nitrogen jet. Slag droplets detach from the slag pool and splash onto the converter liner under a combination of inertial force, drag force, and gravity. The slag droplets spread and form a film on the converter liner surface. In practice, the slag adhered to the converter liner will gradually solidify as the temperature decreases to form a solid slag layer for protecting the refractory.
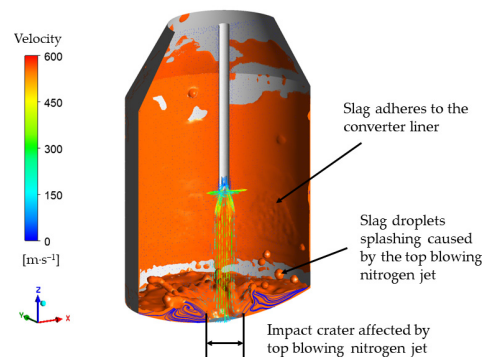
Figure 8. Cross-sectional view of the phase distribution.

Figure 9 displays the morphologies of the splashed slag droplet and the impact crater of the slag pool at different moments. The impact crater morphology of the slag pool is constantly changing. The impact points on the converter liner are determined by the velocity and flow direction of slag droplets detaching from the slag pool.

To better illustrate the distribution of slag on the converter liner, the three-dimensional surface of the converter liner is unfolded into a two-dimensional plane. Figure 10 shows the distribution of slag on the converter liner at different moments. At the start of the splashing process, the slag adhered to the converter liner is unevenly distributed. This inhomogeneity fades away as the splashing time increases. More slag adheres to the lower part of the converter liner, while lesser slag adheres to the upper part of the converter liner and the furnace cap.
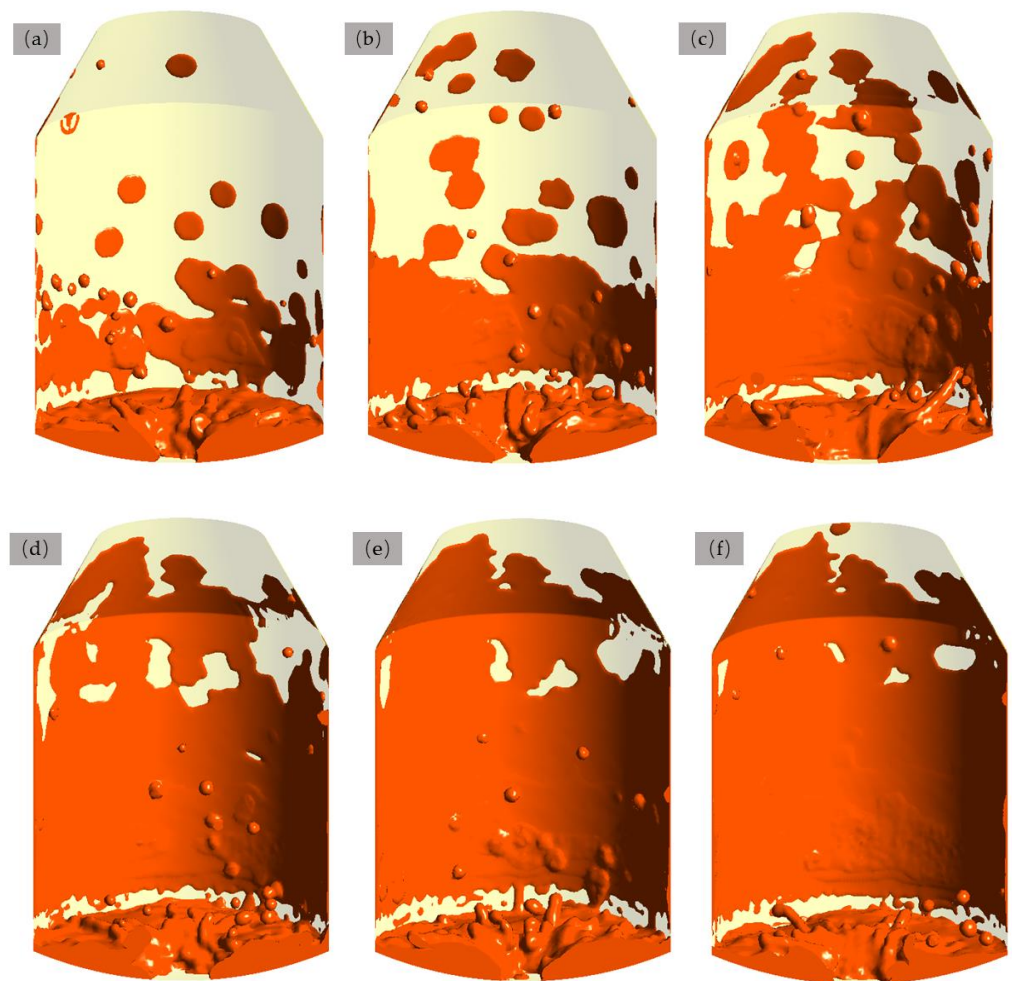
Figure 9. The slag droplets splashing and the impact crater morphology of the slag pool at different moments: (**a**) 5 s, (**b**) 10 s, (**c**) 15 s, (**d**) 20 s, (**e**) 25 s, and (**f**) 30 s.

4.3. Response Surface Analysis

This paper utilizes the Box–Behnken Design (BBD) method of response surface analysis to parametrically analyze the three primary factors that affect the splashing effect: the amount of remaining slag, oxygen lance height, and top-blowing nitrogen flowrate. The BBD analysis, a widely used experimental design method in response surface analysis, is suitable for optimization experiments with 2 to 5 factors. According to the actual experience of the steel mill, the amount of remaining slag range of 120 ton converter for splashing operation is 6~12%, the oxygen lance height range is 1100~1900 mm, and the top-blowing nitrogen flowrate range is 38,000~42,000 Nm$^3\cdot$h^{-1}. Table 4 displays the level and coded values of each factor during splashing. Here, 0 indicates the central experimental point, while +1 and −1 represent the high and low values corresponding to each factor, respectively.

Two indicators are used as evaluation criteria in the response surface analysis of the slag splashing process. One of them is to evaluate the splashing strength using the splashing density. A higher splashing density indicates that more slag droplets fall onto the converter liner per unit time, resulting in more slag adhesion. The other is the splashing area ratio(the proportion of the statistical area of the converter liner covered by slag with a thickness greater than 1 mm to the total statistical area of the converter liner), which indicates the uniformity of slag splashing. Table 5 presents the simulation scheme of the BBD analysis method and the simulation results obtained through numerical calculations.
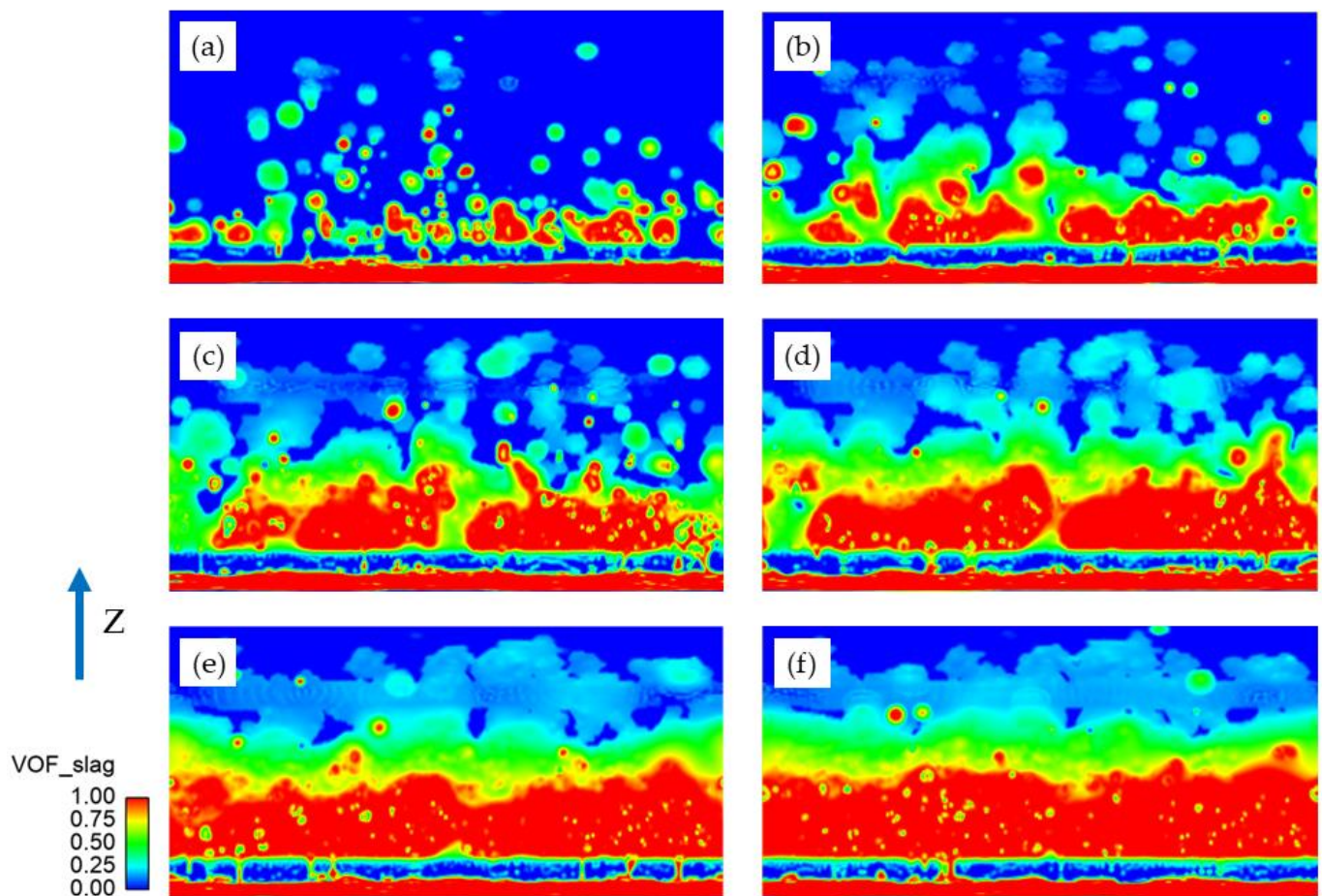
Figure 10. The distribution of slag on the converter liner at different moments: (**a**) 5 s, (**b**) 10 s, (**c**) 15 s, (**d**) 20 s, (**e**) 25 s, and (**f**) 30 s.

Table 4. Code and level of design factors.

Factor	Variable	Level		
		−1	**0**	**1**
Amount of remaining slag/(%)	A	6	9	12
Oxygen lance height/(mm)	B	1100	1500	1900
Top-blowing nitrogen flowrate/(Nm^3 h^{-1})	C	38,000	40,000	42,000

After fitting the obtained data, the quadratic response surface fitted regression equations of the splashing density and the splashing area ratio can be obtained, respectively:

$$Y = -10.9047 - 0.2743A + 0.01186B + 1.62 \times 10^{-4}C - 8.2 \times 10^{-5}AB + 1.7 \times 10^{-5}AC \\ -1.1275 \times 10^{-7}BC - 3.116 \times 10^{-3}A^2 - 2.3865 \times 10^{-6}B^2 - 1.322 \times 10^{-9}C^2 \tag{15}$$

$$Z = -721.4053 + 3.5361A + 0.3422B + 0.02316C + 1.535 \times 10^{-3}AB + 4.33 \times 10^{-4}AC \\ -5.2461 \times 10^{-6}BC - 1.0283A^2 - 5.4 \times 10^{-5}B^2 - 2.1733 \times 10^{-7}C^2 \tag{16}$$

where Y is the splashing density and Z is the splashing area ratio.

Table 6 displays the ANOVA table of the regression equation with the splashing density as the evaluation index. The ANOVA displays that the model is significant and has a good fit, enabling it to accurately represent the relationship between the splashing density and each factor. Larger F-values and smaller *p*-values indicate more significant correlation coefficients. Based on the magnitude of *p*-values, it is evident that the impacts of A, B, and B^2 on the splashing density are significantly significant. Based on the magnitude

of the F-values, the degree of influence on the splashing density is A > B > C, indicating that the splashing density is mainly affected by the amount of remaining slag and the oxygen lance height, the effect of the top-blowing nitrogen flowrate on it is less significant. This is because the size of the oxygen lance nozzle is designed according to the oxygen supply strength required during the blowing process. During the splashing process, the nitrogen flowrate deviates significantly from the oxygen flowrate, leading to the production of expansion and compression waves that can impact the jet performance. This makes the change in jet intensity insignificant when the flowrate of the top-blowing nitrogen jet is changed by a small amount. The order of magnitude of influence on the splashing density is as follows: the amount of remaining slag, oxygen lance height, and top-blowing nitrogen flowrate.

Table 5. Simulation scheme and simulation results of BBD analysis method.

Serial Number	A	B	C	Splashing Density/(kg m^{-2} s^{-1})	Splashing Area Ratio/(%)
1	9	1500	40,000	1.3885	58.5691
2	12	1100	40,000	1.79152	59.6134
3	12	1500	42,000	2.3676	67.9688
4	6	1100	40,000	0.530181	35.5984
5	9	1900	42,000	0.708861	42.4976
6	6	1900	40,000	0.362962	17.9129
7	9	1900	38,000	0.779422	42.0657
8	6	1500	42,000	0.55058	34.53
9	9	1100	42,000	1.40372	64.309
10	9	1500	40,000	1.3885	58.5691
11	9	1500	40,000	1.3885	58.5691
12	9	1500	40,000	1.3885	58.5691
13	6	1500	38,000	0.545771	34.1208
14	9	1100	38,000	1.11349	47.0894
15	12	1900	40,000	1.22979	49.2945
16	12	1500	38,000	1.9567	57.1597
17	9	1500	40,000	1.3885	58.5691

Table 6. ANOVA table for the regression equation (splashing density).

Source	Statistical Analysis					
	Sum of Squares	df	Mean Square	F-Value	*p*-Value	Significance
Model	4.76	9	0.5292	22.15	0.0002	**
A	3.59	1	3.59	150.09	<0.0001	**
B	0.3863	1	0.3863	16.17	0.0051	**
C	0.0505	1	0.0505	2.11	0.1895	
AB	0.0389	1	0.0389	1.63	0.2426	
AC	0.0412	1	0.0412	1.73	0.2304	
BC	0.0325	1	0.0325	1.36	0.2814	
A^2	0.0033	1	0.0033	0.1386	0.7207	
B^2	0.6139	1	0.6139	25.69	0.0014	**
C^2	0.0001	1	0.0001	0.0049	0.9460	
Residual	0.1672	7	40000			
Lack of Fit	0.1672	3	0.0557			
Pure Error	0.0000	4	0.0000			
Cor Total	4.93	16				
R^2	0.9661					
Adjusted R^2	0.9225					

"*" means significant ($p < 0.05$); "**" means extremely significant ($p < 0.01$).

Figure 11 displays a two-factor interaction effect plot with the splashing density as the evaluation index. The figure reveals a positive correlation between the amount of

remaining slag and the splashing density. The more slag left at the bottom of the converter, the higher the number of slag droplets splashed by the top-blowing nitrogen supersonic jet, resulting in a higher splashing density. As the height of the oxygen lance decreases, the splashing density first increases and then decreases. The impact of the top-blowing nitrogen flowrate on the splashing density is relatively small, especially when the oxygen lance height is high, its effect on the splashing density is very insignificant. When the oxygen lance height is low, there is a positive correlation between the top-blowing nitrogen flowrate and the splashing density. Which means, the higher the top-blowing nitrogen flowrate, the higher the splashing density.
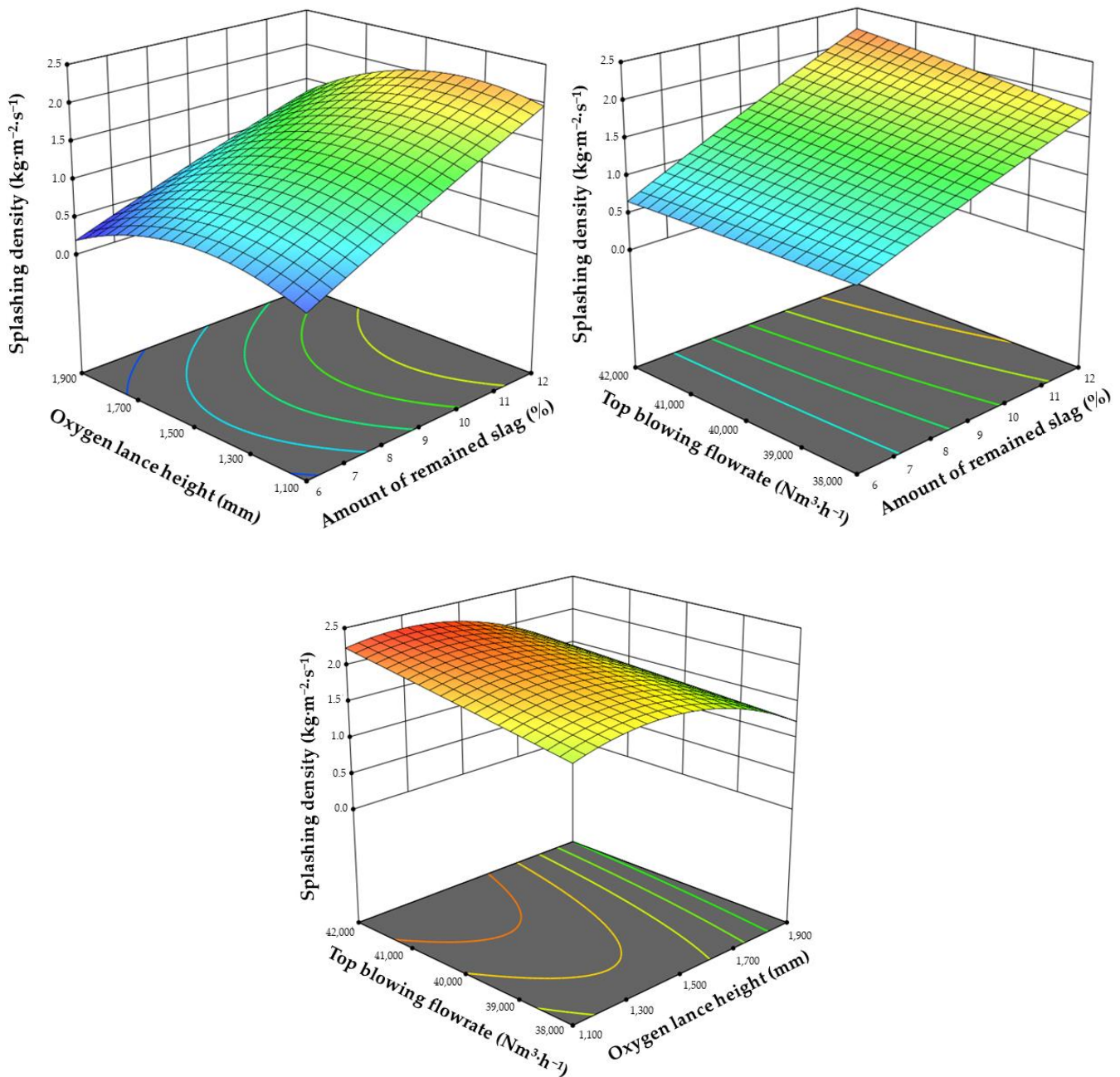
Figure 11. Two-factor interaction effect diagram (splashing density).

As the splashing process is highly dynamic, an increase in splash time results in more and more slag droplets being splashed up by the nitrogen jet. These droplets then spread onto the surface of the converter liner and solidify, resulting in a decrease in the amount of remaining slag left at the bottom of the converter. Figure 12 displays the impact of oxygen

lance height and top-blowing nitrogen flowrate on the splashing density for the amount of remaining slag at 12%, the amount of remaining slag at 9%, and the amount of remaining slag at 6%, respectively. When the amount of remaining slag is larger, the selection range for oxygen lance height and top-blowing nitrogen flowrate becomes more stringent. When the amount of remaining slag is small, the oxygen lance height and the top-blowing nitrogen flowrate have a relatively wide range of selection can ensure a high splashing density.
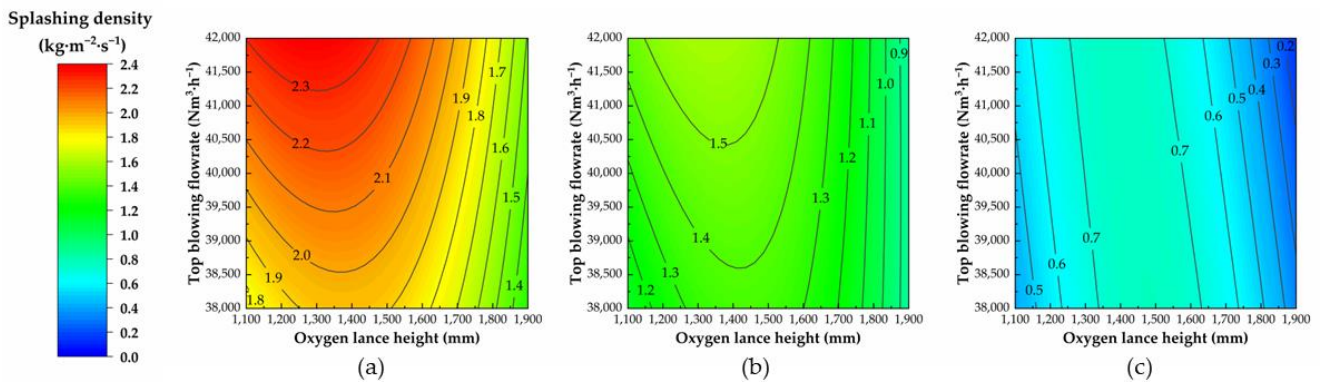
Figure 12. Effect of oxygen lance height and top-blowing nitrogen flowrate on the splashing density with (**a**) the amount of remaining slag at 12%; (**b**) the amount of remaining slag at 9%; (**c**) the amount of remaining slag at 6%.

The top-blowing nitrogen flowrate can be kept at a maximum of 42,000 $Nm^3 \cdot h^{-1}$ during the process of decreasing slag at the bottom of the converter with increasing splashing time. When the amount of remaining slag at the bottom of the converter is high (amount of remaining slag at 12%), the oxygen lance height should be maintained in the range of 1160~1400 mm. After the splashing process has continued for a certain period of time (amount of remaining slag at 9%), the optimal range for oxygen lance height is 1220~1460 mm. When the amount of remaining slag at the bottom of the converter is low (amount of remaining slag at 6%), the optimal range for oxygen lance height is 1280~1540 mm. Overall, to ensure that the splashing density remains at maximum during the splashing slag process, a higher top-blowing nitrogen flowrate is better. The oxygen lance height should be adjusted based on the amount of remaining slag at the bottom of the converter. As the amount of remaining slag at the bottom of the converter decreases gradually, the splashing density increases with an increase in oxygen lance height.

Table 7 displays the ANOVA table of the regression equation with the splashing area ratio as the evaluation index. The ANOVA displays that the model is significant and has a good fit, enabling it to accurately represent the relationship between the splashing area ratio and each factor. Based on the magnitude of p-values, it is evident that the impacts of A, B, C, AB, AC, BC, A^2 and B^2 on the splashing area ratio are significantly significant. Based on the magnitude of the F-values, the degree of influence on the splashing area ratio is A > B > C, indicating that the splashing area ratio is significantly influenced by all three factors. The order of magnitude of influence on the splashing area ratio is as follows: the amount of remaining slag, oxygen lance height, and top-blowing nitrogen flowrate.

Figure 13 displays a two-factor interaction effect plot with the splashing area ratio as the evaluation index. It can be seen from the figure that the amount of remaining slag and top-blowing nitrogen flowrate are positively correlated with the splashing area ratio. As the amount of remaining slag increases, the increase in the splashing area ratio becomes increasingly smooth. As the height of the oxygen lance decreases, the splashing area ratio first increases and then decreases.

Table 7. ANOVA table for the regression equation (splashing area ratio).

Source	Statistical Analysis					
	Sum of Squares	df	Mean Square	F-Value	*p*-Value	Significance
Model	2888.17	9	320.91	409.15	<0.0001	**
A	1564.49	1	1564.49	1994.71	<0.0001	**
B	375.92	1	375.92	479.30	<0.0001	**
C	104.18	1	104.18	132.83	<0.0001	**
AB	13.57	1	13.57	17.30	0.0042	**
AC	27.04	1	27.04	34.48	0.0006	**
BC	70.46	1	70.46	89.83	<0.0001	**
A^2	360.65	1	360.65	459.82	<0.0001	**
B^2	319.38	1	319.38	407.21	<0.0001	**
C^2	3.18	1	3.18	4.06	0.0838	
Residual	5.49	7	0.7843			
Lack of Fit	5.49	3	1.83			
Pure Error	0.0000	4	0.0000			
Cor Total	2893.66	16				
R^2	0.9981					
Adjusted R^2	0.9957					

"*" means significant ($p < 0.05$); "**" means extremely significant ($p < 0.01$).

Figure 14 displays the impact of oxygen lance height and top-blowing nitrogen flowrate on the splashing area ratio for the amount of remaining slag at 12%, the amount of remaining slag at 9%, and the amount of remaining slag at 6%, respectively. When the amount of remaining slag is larger, the selection range for oxygen lance height and top-blowing nitrogen flowrate becomes more stringent. When the amount of remaining slag is small, the oxygen lance height and the top-blowing nitrogen flowrate have a relatively wide range of selection can ensure a high splashing area ratio.

The top-blowing nitrogen flowrate can be kept at a maximum of 42,000 $Nm^3 \cdot h^{-1}$ during the process of decreasing slag at the bottom of the converter with increasing splashing time. When the amount of remaining slag at the bottom of the converter is high (amount of remaining slag at 12%), the oxygen lance height should be maintained in the range of 1200~1400 mm. After the splashing process has continued for a certain period of time (amount of remaining slag at 9%), the optimal range for oxygen lance height is 1170~1350 mm. When the amount of remaining slag at the bottom of the converter is low (amount of remaining slag of 6%), the optimal range for oxygen lance height is 1100~1440 mm. As the amount of remaining slag at the bottom of the converter decreases gradually, the splashing area ratio increases with a decrease in oxygen lance height.

Based on the analysis of the splashing density and the splashing area ratio, it can be concluded that the optimal splashing effect for a 120 ton converter can be achieved within the oxygen lance height range of 1280~1350 mm and a top-blowing nitrogen flowrate of 42,000 $Nm^3 \cdot h^{-1}$.
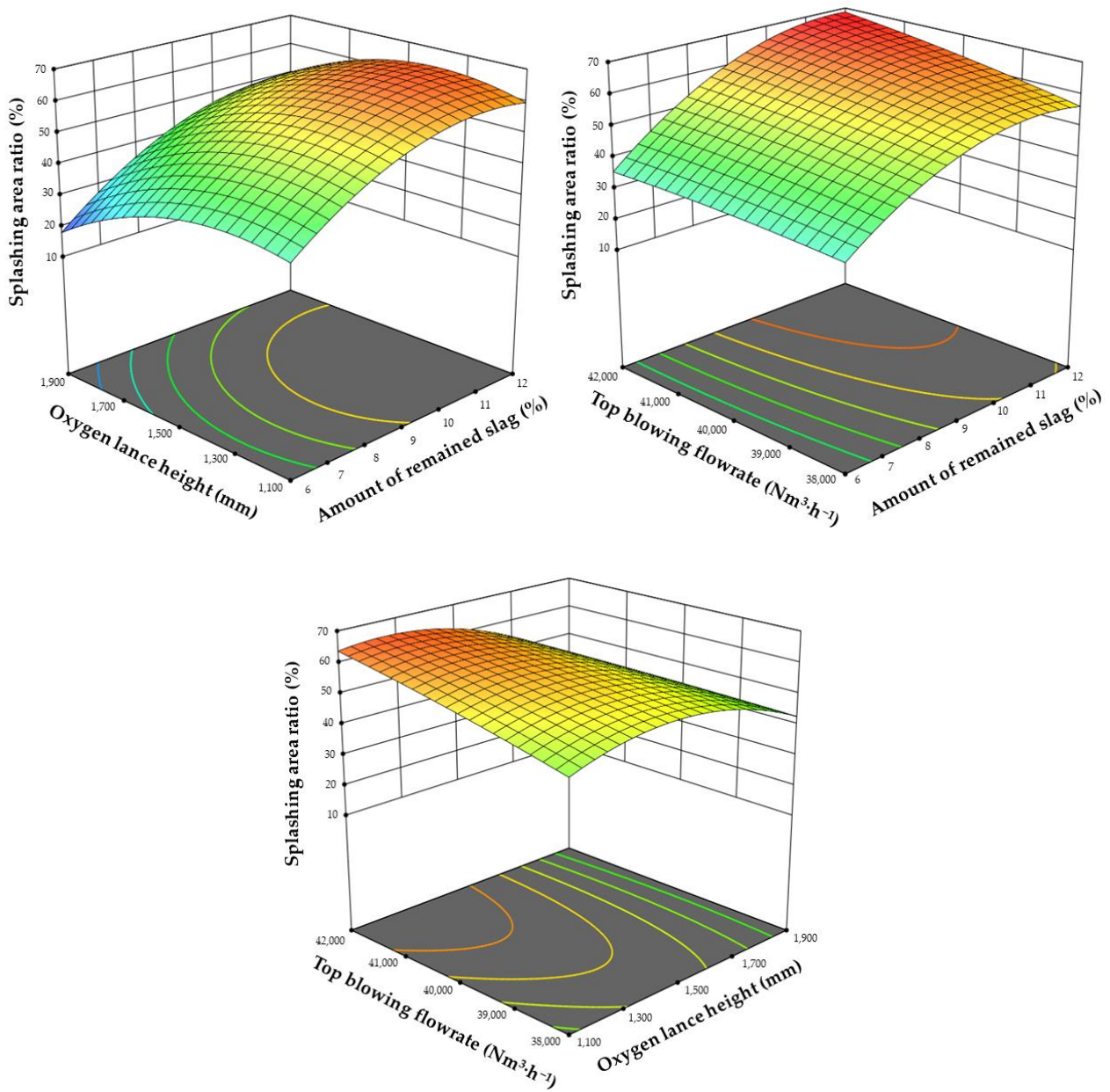
Figure 13. Two-factor interaction effect diagram (splashing area ratio).
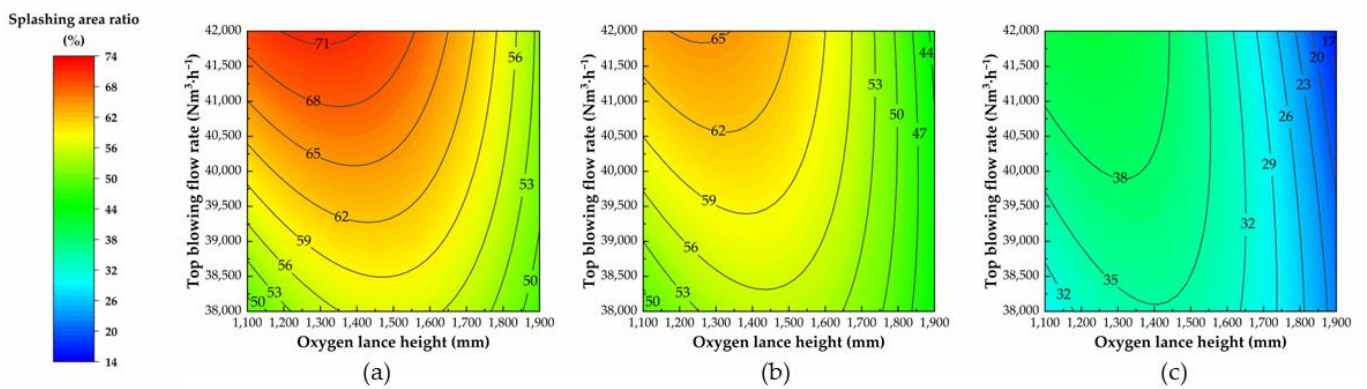
Figure 14. Effect of oxygen lance height and top-blowing nitrogen flowrate on the splashing area ratio with (**a**) the amount of remaining slag at 12%; (**b**) the amount of remaining slag at 9%; (**c**) the amount of remaining slag at 6%.

5. Conclusions

This paper utilizes numerical simulations to perform a response surface analysis of the effects of the amount of remaining slag, oxygen lance height, and top-blowing nitrogen flowrate on slag splashing. The optimal range of operating parameters for the 120 ton converter splashing process is studied and predicted. The main conclusions are obtained as follows:

1. Three factors—the amount of remaining slag, the oxygen lance height, and the top-blowing nitrogen flowrate—are selected to investigate the splash density and the splashing area ratio in the converter liner surface. The splashing density is mainly affected by the amount of remaining slag and the oxygen lance height, while the effect of the top-blowing nitrogen flowrate on the splashing density is less significant. The splashing area ratio is significantly influenced by all three factors. The importance of affecting the splashing density and the splashing area ratio in order is the amount of remaining slag, oxygen lance height, and top-blowing nitrogen flowrate.

2. The splashing density and splashing slag area ratio increase with an increasing amount of remaining slag. As the height of the oxygen lance decreases, the splashing density and the splashing area ratio first increase and then decrease. The top-blowing nitrogen flowrate is positively correlated with the splashing area ratio. When the oxygen lance height is high, the impact of the top-blowing nitrogen flowrate on the splashing density is very insignificant. The splashing density increases with increasing top-blowing nitrogen flowrate when the oxygen lance height is low.

3. When the amount of remaining slag is large, the selection range for oxygen lance height and top-blowing nitrogen flowrate becomes more stringent. When the amount of remaining slag is small, a wide range of parametric selections of the oxygen lance height and the top-blowing nitrogen flowrate can ensure the high splashing density and the splashing area ratio.

4. To maintain the optimal splashing density and the splashing area ratio during the splashing process, a higher top-blowing nitrogen flowrate is recommended. Increasing the oxygen lance height is advised to achieve the optimal splashing density as the slag left at the converter bottom decreases. Reducing the oxygen lance height is encouraged to obtain the optimal splashing area ratio. The optimal splashing effect for a 120 ton converter can be achieved within the oxygen lance height range of 1280~1350 mm and a top-blowing nitrogen flowrate of 42,000 $Nm^3 \cdot h^{-1}$.

The present study analyzes the effects of parameters on the splashing process at actual dimensions and keeps the focus on the influence of each factor on the overall effect of splashing. In actual production, due to the inhomogeneous erosion on the converter liner, it is necessary to splash on a certain region of the converter liner to make the best effect of slag splashing in that part, which will be explored in our future work.

The physical model used in this study is the original size of a 120 ton converter with a four-hole oxygen lance. The outlet of the oxygen lance nozzle may be deformed during the blowing process due to the steel sticking to the oxygen lance and the internal contour of the converter may change as the service time increases. These factors may have some impacts on the effect of slag splashing. For practical production, a good effect of slag splashing is desirable for each service stage of the converter. Hence, the correction of the deformed lance and converter geometry on the splashing effect will be investigated in our future work.

Author Contributions: Conceptualization, G.Y. and B.L.; methodology, G.Y. and B.L.; validation, G.Y., D.Q. and L.Z.; investigation, M.S.; data curation, G.Y. and L.Z.; writing—original draft preparation, G.Y.; writing—review and editing, B.L., M.S. and L.Z.; project administration, B.L.; funding acquisition, B.L. All authors have read and agreed to the published version of the manuscript.

Institutional Review Board Statement: Not applicable.

Informed Consent Statement: Not applicable.

Data Availability Statement: Not applicable.

Conflicts of Interest: The authors declare no conflict of interest.

References

1. Bellemans, I.; Zietsman, J.; Verbeken, K. Fundamental and Formation Aspects of Slag Freeze Linings: A Review. *J. Sustain. Metall.* **2022**, *8*, 64–90. [CrossRef]
2. Zhao, H.; Yuan, Z.; Wu, Y.; Pan, Y.; Li, S.; Qi, T.; Wang, L. Study on thickness control and quantitative of converter lining. *Appl. Mech. Mater.* **2013**, *433–435*, 2156–2163. [CrossRef]
3. Wu, Y.; Gu, J.; Wang, S.; Yuan, Z.; Zhao, H. The application of laser contouring system on converter lining for steelmaking. *Metal. Int.* **2013**, *18*, 8–12.
4. Benoit, T.; Comparini, R.; Coste, M.; Calvo, C.; Cadet, R.; Huber, J. Slag splashing at the Fos steelplant: New converters scheduling and results. *Metall. Res. Technol.* **2005**, *102*, 323–328. [CrossRef]
5. Li, M.; Li, Q.; Kuang, S.; Zou, Z. Computational investigation of the splashing phenomenon induced by the impingement of multiple supersonic jets onto a molten slag-metal bath. *Ind. Eng. Chem. Res.* **2016**, *55*, 3630–3640. [CrossRef]
6. Zhang, B.; Chen, K.; Wang, R.; Liu, C.; Jiang, M. Physical modelling of splashing triggered by the gas jet of an oxygen lance in a converter. *Metals* **2019**, *9*, 409. [CrossRef]
7. Feng, Y.; Gao, J.; Feng, D.; Zhang, X. Modeling of the molten blast furnace slag particle deposition on the wall including phase change and heat transfer. *Appl. Energy* **2019**, *248*, 288–298. [CrossRef]
8. Liu, G.; Li, J.; Xu, D.; Zheng, B. Energy balance between multiple supersonic jets and molten bath in BOF steelmaking. *Ironmak. Steelmak.* **2022**, *49*, 726–736. [CrossRef]
9. Yuan, Z.; Yan, W.; Zhao, H.; Matsuura, H.; Tsukihashi, F. Wettability between Molten Slag and MgO-C Refractories for the Slag Splashing Process. *ISIJ Int.* **2013**, *53*, 598–602. [CrossRef]
10. Chen, L.; Diao, J.; Wang, G.; Qiao, Y.; Xie, B. Experimental study on slag splashing with modified vanadium slag. *Ironmak. Steelmak.* **2019**, *46*, 165–168. [CrossRef]
11. Guo, H.; Yang, J. Research of BOF protection technology by slag splashing. *Mater. Sci. Forum* **2009**, *620–622*, 45–48. [CrossRef]
12. Santos, I.A.S.; Da Silva, A.L.; De Medeiros Santos, V.R.; Dos Reis Lima, W.; Maia, B.T.; De Carvalho, D.A.G. Slag splashing: Blow parameters equationing. In Proceedings of the Iron & Steel Technology Conference 2019, Pittsburgh, PA, USA, 6–9 May 2019; pp. 913–922.
13. Tao, Z.; Li, J.; Jiang, M. Slag splashing technology for 30 t LD converter. *J. Iron Steel Res.* **2005**, *17*, 72–74.
14. Wang, Z.; Liu, Q.; You, L.; Wei, S.; Cao, L. Experimental study on slag splashing of an 80 t combined blown converter. *Ironmak. Steelmak.* **2018**, *45*, 379–385. [CrossRef]
15. Zou, Q.; Hu, J.; Yang, S.; Wang, H.; Deng, G. Investigation of the Splashing Characteristics of Lead Slag in Side-Blown Bath Melting Process. *Energies* **2023**, *16*, 1007. [CrossRef]
16. Mills, K.C.; Su, Y.; Fox, A.B.; Li, Z.; Thackray, R.P.; Tsai, H.T. A review of slag splashing. *ISIJ Int.* **2005**, *45*, 619–633. [CrossRef]
17. Sinelnikov, V.; Szucki, M.L.; Merder, T.; Pieprzyca, J.; Kalisz, D. Physical and numerical modeling of the slag splashing process. *Materials* **2021**, *14*, 2289. [CrossRef]
18. Leão, P.M.G.C.; Rodrigues, E.F.; Da Silva, C.A.; Da Silva, I.A.; Seshadri, V. Influence of physical properties of slag and operational parameters on slag splashing process in an oxygen convertor. In Proceedings of the 10th International Conference on Molten Slags, Fluxes and Salts 2016, Seattle, WA, USA, 22–25 May 2016; pp. 1043–1051.
19. Cao, L.; Liu, Q.; Sun, J.; Lin, W.; Feng, X. Effect of Slag Layer on the Multiphase Interaction in a Converter. *Jom* **2019**, *71*, 754–763. [CrossRef]
20. Zhang, H.; Yuan, Z.; Mei, L.; Peng, X.; Liu, K.; Zhao, H. The Behavior of CO_2 Supersonic Jets in the Converter Slag-Splashing Process. *J. Sustain. Metall.* **2022**, *8*, 1803–1815. [CrossRef]
21. Zhao, H.; Yuan, Z.; Wang, W.; Pan, Y.; Li, S. A novel method of recycling CO_2 for slag splashing in converter. *J. Iron Steel Res. Int.* **2010**, *17*, 11–16. [CrossRef]
22. Sinelnikov, V.O.; Kalisz, D.; Zak, P.L.; Kuzemko, R.D. Power increase of supersonic jets in oxygen converter. *IOP Conf. Series Mater. Sci. Eng.* **2018**, *461*, 012078. [CrossRef]
23. Kalinogorskii, A.N.; Protopopov, E.V.; Chernyatevich, A.G.; Feiler, S.V.; Bagryantsev, V.I. Application of refractory coatings to converter linings by swirling technology. 2. Motion of slag droplets. *Steel Transl.* **2015**, *45*, 923–926. [CrossRef]
24. Zhao, H.; Xiao, Y.; Liu, F.; Sohn, H.Y. Computational fluid dynamics simulation of gas-matte-slag three-phase flow in an ISASMELT furnace. *Metall. Mater. Trans. B* **2021**, *52*, 3767–3776. [CrossRef]
25. Hirt, C.W.; Nichols, B.D. Volume of fluid (VOF) method for the dynamics of free boundaries. *J. Comput. Phys.* **1981**, *39*, 201–225. [CrossRef]
26. Yu, L.; Feng, L.; Nie, D.; Liu, Y. Simulation study on multiphase behavior of gas-metal-slag in the 260t converter. *Met. Res. Technol.* **2022**, *119*, 613–623. [CrossRef]

27. Sun, J.; Zhang, J.; Lin, W.; Cao, L.; Feng, X.; Liu, Q. Effect of Impact Cavity Shape Induced by Supersonic Oxygen Jet on the Dynamic Characteristics of Molten Bath in Converter. *Steel Res. Int.* **2021**, *92*, 2100179–2100188. [CrossRef]

28. Li, M.; Li, Q.; Zou, Z.; An, X. Computational Investigation of Swirling Supersonic Jets Generated Through a Nozzle-twisted Lance. *Metall. Mater. Trans. B* **2017**, *48*, 713–725. [CrossRef]

29. Li, Q.; Li, M.; Kuang, S.; Zou, Z. Understanding Characteristic of Abrasion of Refractory Lining Caused by Bath Oscillation in BOF Steelmaking. *Jom* **2016**, *68*, 3126–3133. [CrossRef]

30. Shih, T.; Liou, W.W.; Shabbir, A.; Yang, Z.; Zhu, J. A new k-ε eddy viscosity model for high Reynolds number turbulent flows. *Comput. Fluids* **1995**, *24*, 227–238. [CrossRef]

31. Zhang, J.; Lou, W.; Shao, P.; Zhu, M. Mathematical Simulation of Impact Cavity and Gas-Liquid Two-Phase Flow in Top-Bottom Blown Converter with Eulerian-Multifluid VOF Model. *Metall. Mater. Trans. B* **2022**, *53*, 3585–3601. [CrossRef]

32. Fuhrman, D.R.; Li, Y. Instability of the realizable k-ε turbulence model beneath surface waves. *Phys. Fluids* **2020**, *32*, 115108–115109. [CrossRef]

33. Kumar, B.; Srivastava, S. Modelling 2-D Supersonic Jet from a Convergent-Divergent Nozzle using k-ε Realizable Turbulence Model. *J. Physics Conf. Ser.* **2019**, *1240*, 012019. [CrossRef]

34. Moen, A.; Mauri, L.; Narasimhamurthy, V.D. Comparison of k-ε models in gaseous release and dispersion simulations using the CFD code FLACS. *Process. Saf. Environ.* **2019**, *130*, 306–316. [CrossRef]

35. Issac, J.; Singh, D.; Kango, S. Experimental and numerical investigation of heat transfer characteristics of jet impingement on a flat plate. *Heat Mass Transf.* **2020**, *56*, 531–546. [CrossRef]

36. Santos, I.A.S.; de Medeiros Santos, V.R.; dos Reis Lima, W.; da Silva, A.L.; Maia, B.T.; de Oliveira, J.R. Slag Splashing: Simulation and analysis of the slags conditions. *J. Mater. Res. Technol.* **2019**, *8*, 6173–6176. [CrossRef]

37. Ubbink, O.; Issa, R.I. A Method for Capturing Sharp Fluid Interfaces on Arbitrary Meshes. *J. Comput. Phys.* **1999**, *153*, 26–50. [CrossRef]